October 2006

Titanium Carbide Derived Nanoporous Carbon for Energy-Related Applications

Ranjan Dash
Drexel University

John Chmiola
Drexel University

Gleb Yushin
Drexel University

Yury Gogotsi
Drexel University

Giovanna Laudisio
University of Pennsylvania

See next page for additional authors

Postprint version. Published in *Carbon*, Volume 44, Issue 12, 2006, pages 2489-2497.
Publisher URL: http://dx.doi.org/10.1016/j.carbon.2006.04.035

Titanium Carbide Derived Nanoporous Carbon for Energy-Related Applications

Abstract
High surface area nanoporous carbon has been prepared by thermo-chemical etching of titanium carbide TiC in chlorine in the temperature range 200–1200 °C. Structural analysis showed that this carbide-derived carbon (CDC) was highly disordered at all synthesis temperatures. Higher temperature resulted in increasing ordering and formation of bent graphene sheets or thin graphitic ribbons. Soft X-ray absorption near-edge structure spectroscopy demonstrated that CDC consisted mostly of sp^2 bonded carbon. Small-angle X-ray scattering and argon sorption measurements showed that the uniform carbon-carbon distance in cubic TiC resulted in the formation of small pores with a narrow size distribution at low synthesis temperatures; synthesis temperatures above 800 °C resulted in larger pores. CDC produced at 600–800 °C show great potential for energy-related applications. Hydrogen sorption experiments at −195.8 °C and atmospheric pressure showed a maximum gravimetric capacity of ~ 330 cm^3/g (3.0 wt.%). Methane sorption at 25 °C demonstrated a maximum capacity above 46 cm^3/g (45 vol/vol or 3.1 wt.%) at atmospheric pressure. When tested as electrodes for supercapacitors with an organic electrolyte, the hydrogen-treated CDC showed specific capacitance up to 130 F/g with no degradation after 10 000 cycles.

Keywords
porous carbon, etching, adsorption, BET surface area, electron microscopy, small angle x-ray scattering

Comments
Postprint version. Published in *Carbon*, Volume 44, Issue 12, 2006, pages 2489-2497.
Publisher URL: http://dx.doi.org/10.1016/j.carbon.2006.04.035

Author(s)
Ranjan Dash, John Chmiola, Gleb Yushin, Yury Gogotsi, Giovanna Laudisio, Jonathan Singer, John E. Fischer, and Sergei Kucheyev

Titanium Carbide Derived Nanoporous Carbon for Energy-Related Applications

Ranjan Dash [a], John Chmiola [a], Gleb Yushin [a], Yury Gogotsi [a,*], Giovanna Laudisio [b], Jonathan Singer [b], John Fischer [b], Sergei Kucheyev [c]

[a] Department of Materials Science and Engineering and A.J. Drexel Nanotechnology Institute, Drexel University, Philadelphia, PA, 19104, USA

[b] Department of Materials Science and Engineering, University of Pennsylvania, Philadelphia, PA, 19104, USA

[c] Lawrence Livermore National Laboratory, Livermore, CA 94550, USA

Abstract

High surface area nanoporous carbon has been prepared by thermo-chemical etching of titanium carbide TiC in chlorine in the temperature range 200–1200°C. Structural analysis showed that this carbide-derived carbon (CDC) was highly disordered at all synthesis temperatures.; Higher temperature resulted in increasing ordering and formation of bent graphene sheets or thin graphitic ribbons. Soft x-ray absorption near-edge structure spectroscopy demonstrated that CDC consisted mostly of sp^2 bonded carbon. Small-angle X-ray scattering and argon sorption measurements showed that the uniform carbon-carbon distance in cubic TiC resulted in the formation of small pores with a narrow size distribution at low synthesis temperatures; synthesis temperatures above 800ºC resulted in larger pores. CDC produced at 600-800°C show great potential for energy-related applications. Hydrogen sorption experiments at -195.8°C and atmospheric pressure showed a maximum gravimetric capacity of ~ 330 cm^3/g (3.0 wt.%). Methane sorption at 25°C demonstrated a maximum capacity above 46 cm^3/g (45 vol/vol or 3.1 wt.%) at atmospheric pressure. When tested as electrodes for supercapacitors with an organic electrolyte, the hydrogen-treated CDC showed specific capacitance up to 130 F/g with no degradation after 10,000 cycles.

Keywords: porous carbon, etching, adsorption, BET surface area, electron microscopy, small angle x-ray scattering

1. Introduction

Porous carbon is undoubtedly the most versatile porous material, not only because of the wide variety of structures that carbon offers but also due to the wide range of applications, ranging from gas storage to molecular sieves, catalyst supports, absorbents, electrodes in batteries and supercapacitors, water/air filters and medical devices [1]. Carbon produced by etching of metal(s) from a metal carbide is called carbide derived carbon (CDC) [2, 3]. It has been experimentally demonstrated that highly porous carbon with tunable pore size can be produced by chlorination of metal carbides, such as B_4C [4], ZrC [5], Ti_3SiC_2 [3, 6], Ti_2AlC [7] and others.

Titanium carbide (TiC) is one of the most common and widely used carbides. It has a rock-salt structure (space group: Fm3m) where the distance between the nearest carbon atoms is 0.4328 nm [8]. Such a small and uniform carbon-carbon distance in the starting material may lead to a highly porous carbon (~56% porosity [2, 3] and 0.56

cm^3/g pore volume calculated assuming conformal transformation) with narrowly distributed small pores. CDC from TiC (henceforth called TiC-CDC) has been reported in the literature [9, 10]. Specific surface area (SSA) increases from 400°C to 1000°C chlorination temperature, followed by a drop at 1200°C. On the other hand the total pore volume remains almost the same for samples chlorinated between 700°C and 1100°C but the the pore size distributions are different. It was also reported that TiC-CDC has an onion-like structure [10]. Previous studies of CDC as supercapacitor electrodes showed high specific capacitance in aqueous H_2SO_4 electrolytes [11, 12]. Formation of CDC from ternary carbides containing Ti has also been reported [3, 6], however to the best of our knowledge no detailed analysis of the TiC-CDC pore structure and pore size distribution has been reported.

This paper describes a parametric study designed to determine the effect of synthesis temperature on porosity, structure and technologically relevant properties of TiC-CDC such as gas storage capacity (hydrogen, methane) and double-layer capacitance.

2. Experimental Section

2.1. Material Synthesis. Titanium carbide powder (formula weight 59.91 g/mol, density 4.93 g/cm^3) with particle size 2 μm was obtained from Alfa Aesar (Stock # 40178). TiC-CDC was synthesized as described elsewhere[2-4]. TiC in a quartz boat was placed in a quartz tube furnace and heated to the desired temperature (200 – 1200°C) under an argon (Airgas, UHP grade) purge. Once the desired temperature was reached, chlorine gas (Airgas, UHP grade) at 10-15 cm^3/min was passed through the 1-inch diameter quartz tube for 3 hours. After chlorination, the furnace was cooled down to room temperature under an argon purge. Selected samples were subjected to additional treatment in hydrogen at 600°C for 2 hours to remove residual chlorine [13].

2.2. Methods. X-ray diffraction (XRD) patterns were collected using a Rigaku diffractometer (λ = 0.154 nm) in stepping mode at 0.05° 2θ for 2 seconds. Raman spectra from 100 to 2000 cm^{-1} were collected using a Renishaw 1000 spectrometer equipped with an Ar^+ laser (λ = 514 nm) at 500X magnification (~2 μm spot size). Analysis was done by fitting the D and G bands of graphite using the fitting application provided by GRAMS 32 software which uses an iteratation of Gaussian and Lorentzian functions. TEM studies were performed using a JEOL 2010F microscope at 200kV. Samples were prepared by dispersing CDC in isopropyl alcohol over a copper grid with a lacey carbon film.

Soft x-ray absorption near-edge structure (XANES) spectroscopy was performed using the Advanced Light Source undulator beamline 8.0 at Lawrence Berkeley National Laboratory. . Spectra were obtained from total electron yield measurements by monitoring the total sample photocurrent. The incoming radiation flux was monitored by measuring the total photocurrent produced in a highly transmissive Au mesh inserted into the beam. All XANES spectra were normalized to the Au mesh photocurrent. The monochromator was calibrated by aligning the π* resonance in the carbon K-edge of highly oriented pyrolytic graphite (HOPG) to 285.4 eV. After a linear background subtraction, all spectra were normalized to the post-edge step heights.

Gas sorption analysis was done using Quantachrome Autosorb-1 with argon and hydrogen adsorbates at -195.8°C and methane at 25°C. Argon sorption analysis at -195.8°C was used for calculating specific surface area (SSA) using the Brunauer-Emmet-Teller (BET) equation and non-local density functional theory (NLDFT) [14-17]. Pore size distributions (PSD) and pore volumes were determined using the NLDFT method provided by Quantachrome's data reduction software (version 1.27) for Ar isotherms collected at -195.8°C [14]. In contrast to classical thermodynamic methods for PSD calculations, the NLDFT method is based on a statistical mechanics model, and calculations depend on the absorbate-absorbent system. Classical thermodynamic theories like Barrett-Joiner-Halenda (BJH) are based on pore condensation and thus are only applicable to mesopores. Dubinin-Radushkevich (DR), Horvath and Kawazoe (HK), and Saito and Foley (SF) methods are based on continuous pore filling and thus are applicable to micropores only. For a material having both micropores and mesopores, BJH, DR, HK and SF methods cannot accurately describe the PSD and thus we selected NLDFT for the present study. Despite many advantages, it is important to note that the Quantachrome version assumes slit-shaped pores with pore walls of carbon having the same density, and the adsorbate is considered as a fluid of hard spheres [14]. The CDC weighted pore size was calculated as $\frac{\sum_{i=1}^{n} d_i . v_i}{\sum_{i=1}^{n} v_i}$ where d and v are pore width and volume respectively. Hydrogen gravimetric density (wt.%) was defined as $\left(\rho_{Hydrogen} . v_{Hydrogen} . 100\right)$, where $\rho_{Hydrogen}$ is the hydrogen density in g/cm^3 and $v_{Hydrogen}$ is the volume of hydrogen (cm^3/g) adsorbed at -195.8°C and ~760 mm Hg per unit mass of TiC-CDC. Methane gravimetric density of (wt.%) was defined as $\left(\rho_{Methane} . v_{Methane} . 100\right)$, where $\rho_{Methane}$ is the methane density in g/cm^3 and $v_{Methane}$ is the volume of methane (cm^3/g) adsorbed at 25°C and ~760 mm of Hg per unit mass of TiC-CDC. The volume ratio of methane to TiC-CDC (referred as vol/vol) was defined as $\left(\rho_{CDC} . v_{Methane}\right)$, where ρ_{CDC} = 0.98 g/cm^3, the theoretical apparent density of TiC-CDC [6].

Small-angle X-ray scattering (SAXS) experiments were performed on a multi angle diffractometer equipped with a Cu rotating anode, double-focusing optics, evacuated flight path and a two-dimensional wire detector. Powder samples, heated at 80ºC overnight, were loaded and sealed in 1 mm-diameter glass capillaries and measured in transmission for 1h. Data was collected over a Q range of 0.02-1.00Å^{-1}. The scattering intensity from an empty capillary was collected and subtracted with the sample absorption corrected. After subtraction of the empty capillary intensity, a residual flat backround was found to affect the high Q range.

Cyclic voltammery and galvanostatic charge-discharge were performed on electrodes produced from TiC-CDC in 1.5 M tetraethylammonium tetrafluoroborate in acetonitrile using a Solartron 1287 potentiostat/galvanostat. Electrodes were produced by combining 95% CDC and 5% PTFE (E.I. du Pont de Nemours, Wilmington, DE) to from a pliable mass which was then rolled to a ~150 μm thick foil as described elsewhere [11]. Electrodes were dried overnight in vacuum at 80ºC. Two-electrode

cells were assembled in an airtight glovebox with 2 TiC-CDC electrodes sandwiching a porous polypropylene separator. Specific capacitance was calculated from the discharge curves at 1 mA using the equation: $C = \frac{-2i}{m\ dV/dt}$, where m is the mass of a single electrode, i is the discharge current and dV/dt is the slope of the discharge curve. All voltages were referenced to the open cell voltage of the fully discharged cell.

3. Results and Discussion

3.1. CDC Structure

Powder XRD data (Fig. 1) shows that the complete conversion of titanium carbide to carbon takes place at 400°C and higher. The absence of sharp peaks corresponding to graphite, even at 1200°C, indicates the disordered nature of TiC-CDC. Thus it can be called "amorphous carbon".

The Raman spectra of perfectly ordered graphite shows only one peak in the range studied, the G band corresponding to in-plane stretching at 1582 cm^{-1}. Disordered carbons generally exhibit a second disorder-induced (D) peak at ~1350 cm^{-1}, which is generally associated with a double-resonance effect [18]. Raman analysis of TiC-CDC showed two peaks corresponding to the D and G bands of graphitic carbon (Fig. 2a). The width and intensity of these two peaks suggest the disordered nature of carbon produced from TiC. However, increasing the chlorination temperature resulted in decreasing the full-width at half maximum (FWHM) of the D and G bands (Fig. 2b). The sharp decrease between 800 and 1000°C indicates a substantial increase in carbon ordering at 1000°C and above.

Fig. 3 gives a comparison of carbon K-edge XANES spectra of graphite, diamond, and CDCs prepared at different temperatures. These spectra reflect angular-momentum-selected electronic transitions from the carbon 1s core level to the conduction band. Hence, if possible core-hole relaxation, electron correlation effects and higher multipole transitions are ignored, spectra in Fig. 3 essentially map the p-projected density of empty carbon-related states above the Fermi level [19].

Spectra of TiC-CDCs in Fig. 3 exhibit three major peaks centered at ~285.4, ~288.5, and ~291.8 eV. The strong peak at ~285.4 eV is assigned to the $1s \rightarrow \pi^*$ transition of sp^2-bonded carbon, and the broad peak at ~292 eV is related to the σ bonds of sp^2-bonded carbon [19]. The high intensity of these sp^2-related π^* and σ^* peaks clearly demonstrates that sp^2-type bonding is dominant in these materials. No features of sp^3-bonded C can be seen in spectra of CDCs in Fig. 3, as evidenced by the absence of the diamond related peak at ~289.2 eV and a dip at ~302 eV.

The third major peak centered on ~288.5 eV in spectra of CDCs can be attributed to C=O bonds and is related to oxygen contamination. The precise energy position of the π^*C=O-related peak depends on the specific environment of the carbon atoms in the double bonds (see, for example, [20]). However, our assignment of this peak to residual oxygen is based on the correlation of its relative intensity with the intensity of peaks in the second order oxygen K-edge at ~272 eV (not shown). The presence of chemically bonded oxygen could be explained by dangling bonds formed at low temperatures and oxygen-passivated by atmospheric exposure. EDS analysis showed up to 3.4 wt.% oxygen [6].

TEM images (Fig. 4) show a gradual structural evolution with increasing chlorination temperature. At temperatures (400°C), the CDC consists of amorphous carbon with no detectable graphene layers (Fig. 4a). At 800°C (Fig. 4b), CDC is organized into highly curved graphene sheets (open fullerene-like structure). Above 800°C, curved thin graphitic ribbons with interplanar spacing ~0.34 nm can be distinguished in the micrographs (Fig. 4c,d). Amorphous carbon is still present but in a considerably smaller quantity.

XRD, Raman spectra and TEM all show that TiC-CDC is a disordered graphitic carbon. It is X-ray amorphous, but Raman spectroscopy and TEM show that gradual ordering has taken place with increasing chlorination temperature. The low degree of ordering in TiC-CDC produced at temperatures up to 1200°C suggests that the ribbons are interlocked and cannot rearrange themselves into an ordered graphitic state (e.g., thick graphite ribbons or graphite nanocrystals). This behavior is similar to what is observed in CDC produced from ZrC [5], which like TiC has a rock-salt structure.

3.2. Surface Area and Porosity Measurements

3.2.1. Sorption analysis

Argon sorption isotherms (Fig. 5a) collected for different synthesis temperatures show that the volume of argon adsorbed at a relative pressure (P/P^0) of ~1 increases with synthesis temperature. No hysteresis was observed between adsorption and desorption isotherms for samples synthesized at 1000°C and below, indicating the microporous nature (pores less than 2 nm) of these carbons. Hysteresis was observed from samples synthesized at 1200°C, indicating the presence of mesopores (pores greater than 2 nm). The same data plotted on a semilogarithmic scale. Fig. 5b shows that the 800°C sample has the highest Ar sorption at a relative pressure below 10^{-5}, which implies the highest volume of smaller pores compared to samples synthesized at other temperatures. Fig 5b also shows an increase in argon sorption at low relative pressure after hydrogen treatment, indicating increased numbers or accessibility of small pores.

PSDs of TiC-CDC synthesized at 400 and 600°C (Figs. 6d, e) show that the carbon contains narrowly distributed micropore sizes. At 800°C (Fig. 6c), the PSD exhibits slight broadening with a simultaneous shift of the distribution maximum towards smaller pores. The volume of mesopores remains very small (Fig. 6h). With further increase in synthesis temperature (1000 and 1200°C) (Figs. 6a, b), the mesopore volume increases to ~0.5 cm^3/g at 1200°C while the micropore volume decreased to 0.4 cm^3/g. Fig. 6f shows that the weighted average pore size gradually increases with synthesis temperature. The BET SSA (Fig. 6g) increased from ~1200 m^2/g at 400°C to a maximum of ~1800 m^2/g at 1000°C. The NLDFT SSA showed similar trends. Graphitization at higher temperatures results in a small decline in SSA. Purging with hydrogen at 600°C removes residual chlorine and increases both SSA (Fig. 6g) and micropore volume (Fig. 6h).

Both TiC and ZrC are group-IV metal carbides with the same fcc crystal structure and similar lattice constants, thus similar C-C neighbor distances. These similarities may explain why the corresponding PSDs are so similar [5]. However, similar trends in structure development, including enhanced graphitization and pore broadening at > 1000°C, were observed for other carbides as well [6].

3.2.2. Small angle X-ray scattering

SAXS profiles are shown in Fig. 7. For synthesis temperatures up to 800ºC, three Q regimes can be identified. Two power-law regimes with similar exponents at low and high Q are separated by a region of almost constant intensity. For chlorination temperatures above 800º, the plateau at intermediate Q becomes a shoulder of the high Q power law regime which shifts to lower Q with increasing chlorination temperature. From the PSDs (Fig. 6 a-e) we expect micropores to dominate in the range 400-800ºC. This suggested analysis using a two-phase model first proposed by Kalliat *et al.* [21] and modified by Gibaud *et al*.[22]. It assumes an arbitrary admixture of macro and micropores, where the macropores are presumably so large that their Guinier regime lies below the low-Q cutoff of the experiment.

The approach proposed by Gibaud *et al.* relates the scattered intensity profile *I(Q)* to the total surface areas of macro (A) and micropores (B) plus a background C:

$$I(Q) = \frac{A}{Q^4} + \frac{B}{(\frac{6}{R_g^2} + Q^2)^2} + C \qquad (1)$$

where R_g is the micropore radius of gyration. Both macro and micropores are assumed monodisperse, i.e intermediate sizes are excluded. If only micropores are present, the first term (low Q) can be identified with Porod-like or fractal scattering from *external* surfaces of particles comprising the sample. This limit applies well to 400ºC - 600ºC TiC-CDCs (lower curves in Fig. 7); the corresponding PSDs indicate no large pores and the low-Q slope is ~ 3.8, close to the ideal Porod slope 4 for smooth particles. At higher Q, up to $QR_g \le \sqrt{6}$, *I(Q)* remains relatively constant. The plateau upper limit $QR_g = \sqrt{6}$ defines the micropore R_g and demarcates a crossover to a second power-law regime at higher Q representing scattering from *internal* micropore surfaces.

Fits to Eq. (1) confirm the qualitative observation that the constant intensity plateaus encompass different Q ranges as the chlorination temperature increases from 400ºC, first shifting to slightly higher Q at 600ºC and then to much lower Q at 800ºC. Accordingly, the fitted R_g values exhibit a minimum at 600ºC, in agreement with PSD-based average pore sizes in Fig. 6f. The SAXS profiles at 1000ºC and 1200ºC are qualitatifvely different; the plateau is no longer obvious, the low Q scattering becomes more intense relative to the micropore contribution at higher Q, and the exponent of the low Q power law is drastically reduced from ~ 3.8 to ~2. In particular, the smearing of the $QR_g = \sqrt{6}$ crossover suggests the onset of micropore formation with a distribution of R_gs at higher temperature, consistent with the PSDs in Figs. 6a and 6b. Furthermore, the evolution of the plateau regime into a shoulder at low Q is consistent with the formation of mesopores with $Rg > 2\pi/Q_{min}$ where Q_{min} is the instrumental cutoff. The increasing intensity in the range $0.04 < Q < 0.2$ suggests an increasing mesopore contribution with increasing temperature, as in Fig. 6g. Fig. 7 also shows that H_2 annealing has little effect on the SAXS profiles at 400ºC and 800ºC, indicating no major change in structure.

3.3. Energy Related Applications

High SSA, pore volume and tunable pore size are the key structural features that make CDC potentially useful in a number of applications in which porous carbons are currently used. We investigated some properties of TiC-CDCwhich are important for applications in electrochemical energy storage and gas storage applications.

3.3.1. Electrochemical measurements

Cyclic voltammetry measurements (Fig. 8a) on TiC-CDC do not show any major Faradic reactions within a large voltage window of 4 V. These would appear as peaks on the hysteresis loop, and would be detrimental to electrode performance. The gravimetric specific capacitance varies with synthesis temperature, and reaching a maximum of 130 F/g at a synthesis temperature of 600ºC. The volumetric capacitance was in excess of 115 F/cm^3. These values are among the highest reported [23], highlighting the effectiveness of CDC in electrochemical energy storage applications. Cycling data show that the specific capacitance does not change appreciably after 10,000 full charge-discharge cycles between 0 and 2V (Fig. 8b). TiC-CDC also exhibit high gravimetric and volumetric capacitance in aqueous electrolytes, with maximum values for at 800^{o}C synthesis temperature [12].

3.3.2. Hydrogen sorption at 77K

Hydrogen sorption isotherms are shown in Fig. 9 (semilog scale). Samples synthesized at 400°C, 600°C 800°C, and 1000^{o}C follow almost the same path at pressures below 2 mm Hg (point labeled A). Between 2 and 60 mm Hg (from A to B) the amount of hydrogen adsorbed/desorbed is similar for CDCs synthesized at 600°C and 800°C and separately for CDCs synthesized at 400°C and 1000°C. Sorption at low pressures is generally governed by filling the smallest pores, so the observed similarities are consistent with similarities in the PSDs; the volume of pores smaller than 0.5 nm is similar for samples produced at 600°C and 800°C as well as for 400°C and 1000^{o}C samples (data not shown).

We previously showed a clear correlation between micropore volume and hydrogen uptake in CDC produced from B_4C [24]. For TiC-CDC, we find a strong correlation between DFT SSA for pores less than 0.5 nm (dotted line in inset of Fig. 8) and hydrogen uptake (inset in Fig. 9). Thus, carbon materials with small pores are highly favorable for optimizing hydrogen uptake [24]. The 1200^{o}C sample has larger pores and a smaller volume of pores < 0.5 nm, which we believe accounts for the reduced sorption of hydrogen. A hydrogen storage capacity of 2.8 wt% (TiC-CDC chlorinated at 800^{o}C) is twice that of MOF-5 [25, 26] and several times higher than that of SWCNT [27] or MWCNT, all at 77K and 1 atm.. CDC performance can be further improved by treating the sample in hydrogen to remove residual chlorine from the pores. This has the effect of making the pores more accessible, and the capacity can be thereby increased to 3 wt.% (Fig.. 9).

3.3.3. Methane sorption at room temperature.

Like hydrogen sorption, high micropore volumes and narrow PSDs favor higher methane sorption (Fig.10). In spite of different molecular size and temperature of the experiment, hydrogen and methane sorption dependences on the synthesis temperature

are similar (compare Fig. 9 and 10). As the sample synthesized at 800°C has the highest micropore volume, the amount of methane uptake was the highest. The 1200°C sample has a lower micropore volume, larger pore size and broader PSD, resulting in the lowest methane uptake.

The methane sorption at 25°C and atmospheric pressure for samples synthesized at 800°C and corresponds to 45 vol/vol, which is 25% of DOE's target of 180 vol/vol required at a pressure up to 34.5 atm (35 bar) and 25°C. TiC-CDC prepared at 800°C showed higher methane uptake than activated carbon (< 35 cm^3/g) [28] and metal organic framework (IRMOF-6)(< 10 cm^3/g) [29] at 25°C and atmospheric pressure.

4. Conclusion

The small and uniform C-C distance in the precursor TiC results in a nanoporous carbon with narrow PSD and amorphous structure at low synthesis temperatures (400 and 600°C). Increasing the synthesis temperature to 800°C and above results in more ordered carbon structure with larger pores and broader PSD. Nanoporous CDC consists mostly of sp^2 bonded carbon. The TiC crystal structure and high theoretical density of the resulting CDC might be responsible for interlocking of carbon ribbons which imhibits extensive graphitization at temperatures up to 1200°C.

Testing of the produced porous carbon for gas storage as well as for electrochemical energy storage applications, demonstrated its excellent performance. The hydrogen storage at ambient pressure for untreated CDCs varied from 1.4 wt% to 2.8 wt%. The highest methane uptake was 46 cm^3/g (3.1 wt.%) at 25°C and atmospheric pressure. When used as electrodes in supercapacitors with organic electrolyte, no degradation was seen after 10,000 cycles and the capacitance was 130 F/g and 115 F/cm^3.

5. Acknowledgements

This work was supported in part by Arkema, France, and the U.S. Department of Energy contract DE-FC36-04GO14282. XANES experiments were performed at the Advanced Light Source, Lawrence Berkeley National Laboratory under the auspices of the U.S. DOE by the University of California, LLNL under Contract No. W-7405-Eng-48. The ALS is supported by the Director, Office of Science, Office of BES, Materials Sciences Division, of the U.S. DOE under Contract No. DE-AC03-76SF00098 at LBNL.

6. References

[1] Schuth, F, Sing, SWK, Weitkamp, J, Handbook of Porous Solids. In: Schuth, F.; Sing, S. W. K.; Weitkamp, J., editor. Handbook of Porous Solids, vol 4, Wiley-VCH: 1766-1960

[2] Nikitin, A, Gogotsi, Y, Nanostructured Carbide-Derived Carbon (CDC). In: Nalwa, H. S., editor. Encyclopedia of Nanoscience and Nanotechnology, vol 7, CA; American Scientific Publishers: 553-574

[3] Yushin, G, Nikitin, A, Gogotsi, Y, Carbide Derived Carbon. In: Gogotsi, Y., editor. Handbook of Nanomaterials, CRC Press: 237-280

[4] Dash, RK, Nikitin, A, Gogotsi, Y, Microporous Carbon Derived From Boron Carbide. Microporous and Mesoporous Materials 2004; 72; 203-208.

[5] Dash, RK, Yushin, G, Gogotsi, Y, Synthesis, Structure and Porosity Analysis of Microporous and Mesoporous Carbon Derived from Zirconium Carbide. Microporous and Mesoporous Materials 2005; 86; 50-57.
[6] Gogotsi, Y, Nikitin, A, Ye, H, Zhou, W, Fischer, JE, Yi, B, et al., Nanoporous Carbide-Derived Carbon with Tunable Pore Size. Nature Materials 2003; 2; 591-594.
[7] Hoffman, EN, Yushin, G, Barsoum, MW, Gogotsi, Y, Synthesis of Carbide-Derived Carbon by Chlorination of Ti_2AlC. Chemistry of Materials 2005; 17; 2317-2322.
[8] Pierson, HO, Handbook of Refractory Carbides and Nitrides. William Andrew Publishing/Noyes. 1996: 340
[9] Fedorov, NF, Ivakhnyuk, GK, Gavrilov, DN, Porous Structure of Carbon Adsorbents from Titanium Carbide. Zhurnal Prikladnoi Khimii 1982; 55, (1); 46-50.
[10] Zheng, J, Eckström, TC, Gordeev, SK, Jacob, M, Carbon with an Onion-Like Structure Obtained by Chlorinating Titanium Carbide. Journal of Material Chemistry 2000; 10; 1039-1041.
[11] Chmiola, J, Yushin, G, Dash, RK, Hoffman, EN, Fischer, JE, Barsoum, MW, et al., Double-Layer Capacitance of Carbide Derived Carbons in Sulfuric Acid. Electrochemical and Solid State Letters 2005; 8, (7); A357-A360.
[12] Chmiola, J, Dash, RK, Yushin, G, Gogotsi, Y, Effect of Pore Size and Surface Area of Carbide Derived Carbons on Specific Capacitance. Journal of Power Sources, in press.
[13] Erdemir, A, Kovalchenko, A, McNallan, MJ, Welz, S, Lee, A, Gogotsi, Y, et al., Effects of High-Temperature Hydrogenation Treatment on Sliding Friction and Wear Behavior of Carbide-Derived Carbon Films. Surface & Coatings Technology 2004; 188–189; 588–593.
[14] Ravikovitch, PI, Neimark, AV, Characterization of Nanoporous Materials from Adsorption and Desorption Isotherms. Colloids and Surfaces 2001; 187–188; 11–21.
[15] Brunauer, S, Emmett, P, Teller, E, Adsorption of Gases in Multimolecular Layers. J. of American Chemical Society 1938; 60; 309–319.
[16] Gregg, SJ, Sing, KSW, Adsorption, Surface Area and Porosity. London: Academic Press. 1982: 42–54
[17] Lowell, S, Schields, JE, Powder Surface Area and Porosity. New York: 1998: 17-29
[18] Ferrari, AC, Robertson, J, Interpretation of Raman spectra of Disordered and Amorphous Carbon. Physical Review Letters 2000; B61; 14095–14107.
[19] Stöhr, J, NEXAFS Spectroscopy. Berlin: Springer. 1996:
[20] Urquhart, SG, Ade, H, Trends in the Carbonyl Core (C 1S, O 1S) → π*C=O Transition in the Near-Edge X-ray Absorption Fine Structure Spectra of Organic Molecules. Journal of Physical Chemistry B 2002; 106; 8531.
[21] Kalliat, M, Kwak, CY, Schmidt, PW, In New Approaches in Coal Chemistry. American Chemical Society: Washington, DC, 1981.
[22] Gibaud, A, Xue, JS, Dahn, JR, A Small-Angle X-ray Scattering Study of Carbons Made from Pyrolyzed Sugar. Carbon 1996; 34, (4); 499-503.
[23] Burke, A, Ultracapacitors: Why, How, and Where Is the Technology? J. Power Sources 2000; 91; 37-50.
[24] Gogotsi, Y, Dash, RK, Yushin, G, Yildirim, T, Laudisio, G, Fischer, JE, Tailoring of Nanoscale Porosity in Carbide-Derived Carbons for Efficient Hydrogen Storage. Journal of American Chemical Society 2005; 127, (46); 16006–16007.

[25] Lee, J, Li, J, Jagiello, J, Gas Sorption Properties of Microporous Metal Organic Frameworks. Journal of Solid State Chemistry 2005; 178; 2527-2532.
[26] Kaye, SS, Long, JR, Hydrogen Storage in the Dehydrated Prussian Blue Analogues M3[Co(CN)6]2 (M = Mn, Fe, Co, Ni, Cu, Zn) Journal of American Chemical Society 2005; 127; 6506-6507.
[27] Anson, A, Callejas, MA, Benito, AM, Maser, WK, Izquierdo, MT, Rubio, B, et al., Hydrogen Adsorption Studies on Single Wall Carbon Nanotubes. Carbon 2004; 42; 1243–1248.
[28] Lozano-Castello, D, Cazorla-Amoros, D, Linares-Solano, A, Quinn, DF, Influence of Pore Size Distribution on Methane Storage at Relatively Low Pressure: Preparation of Activated Carbon with Optimum Pore Size. Carbon 2002; 40, (7); 989.
[29] Eddaoudi, M, Kim, J, Rosi, N, Vodak, D, Wachter, J, O'Keeffe, M, et al., Systematic Design of Pore Size and Functionality in Isoreticular MOFs and Their Application in Methane Storage. Science 2002; 295, (5554); 469-472.

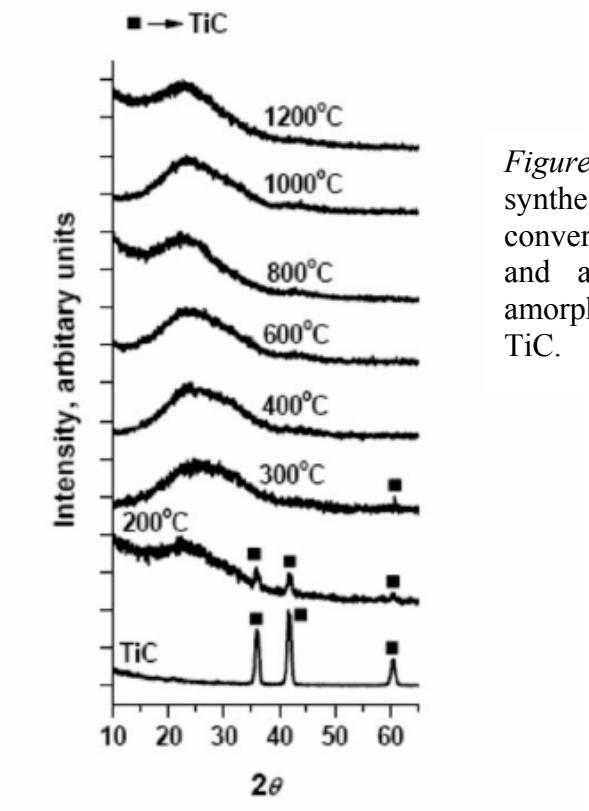

Figure 1. XRD of TiC and TiC-CDC samples synthesized at different temperatures. Complete conversion of TiC to carbon takes place at 400°C and above. Broad peaks show the highly amorphous nature of the carbon produced from TiC.

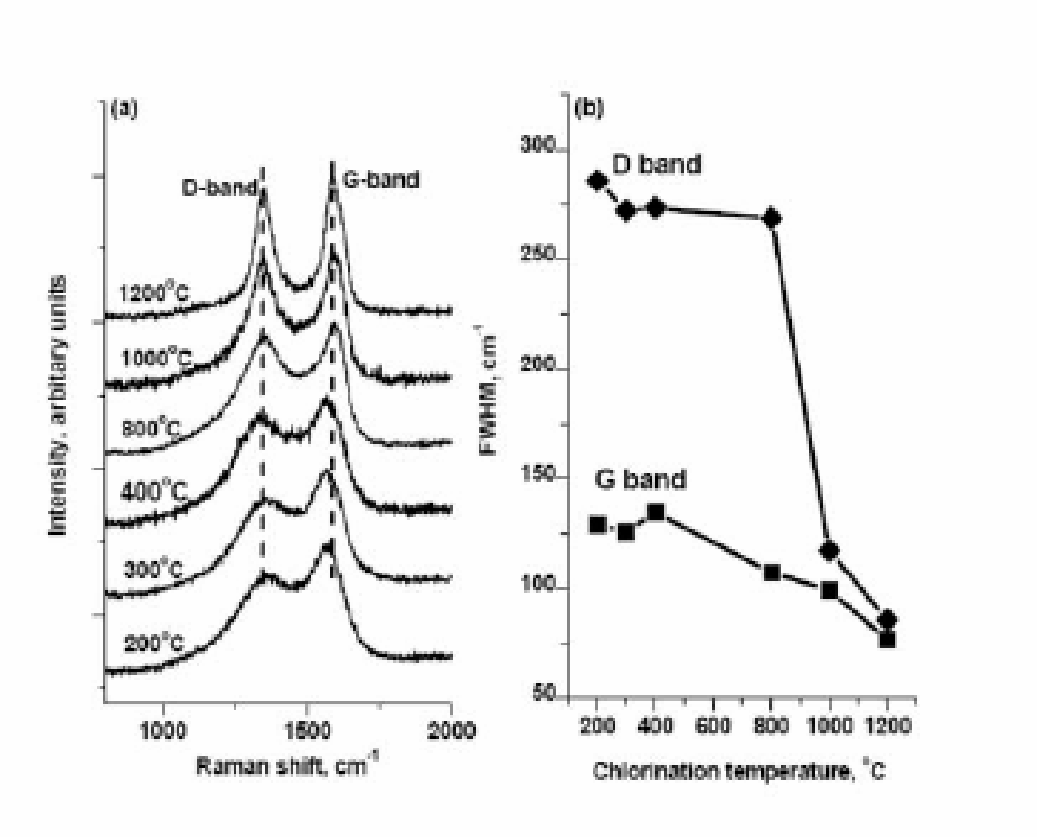

Figure 2. a) Raman spectra of samples synthesized at different temperatures. b) FWHM of D and G bands. Narrowing of D and G bands with increase in synthesis temperature indicates the structural ordering of carbon.

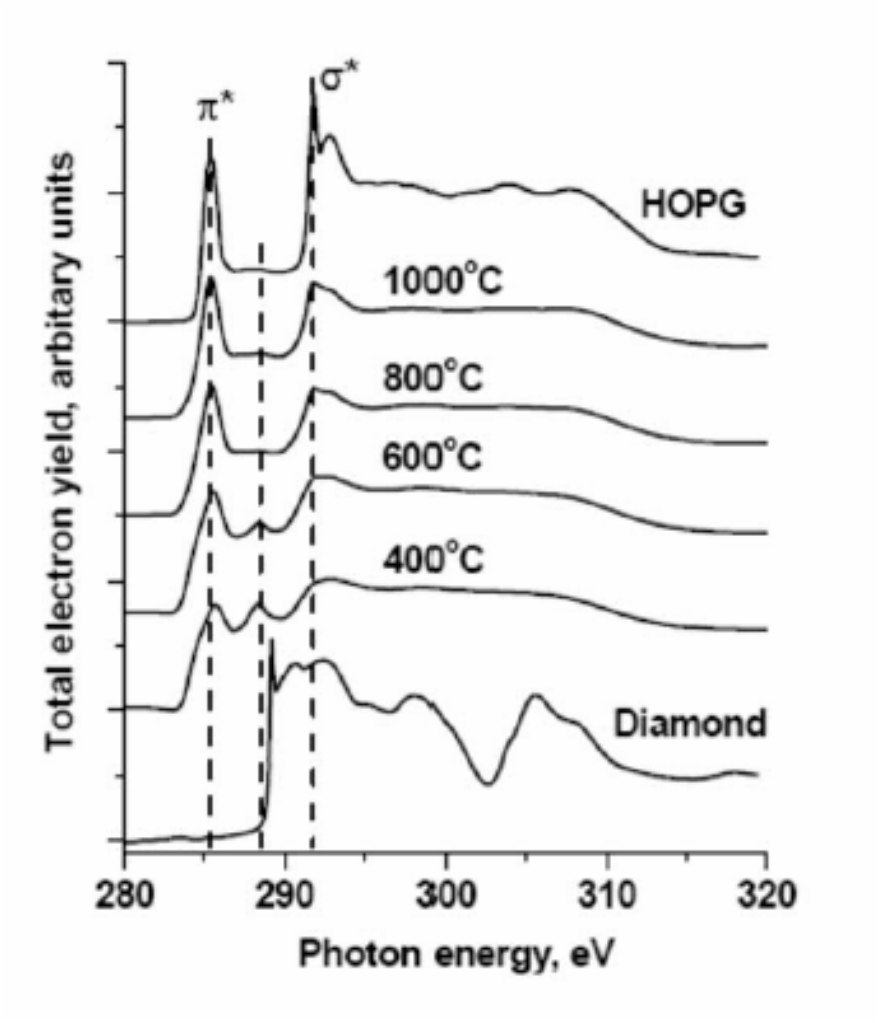

Figure 3. Carbon K-edge XANES spectra of a clean type IIB conducting diamond (111) single crystal, highly oriented pyrolytic graphite (HOPG), and TiC-CDCs prepared at different temperatures. CDC samples consist mostly of sp^2 bonded carbon.

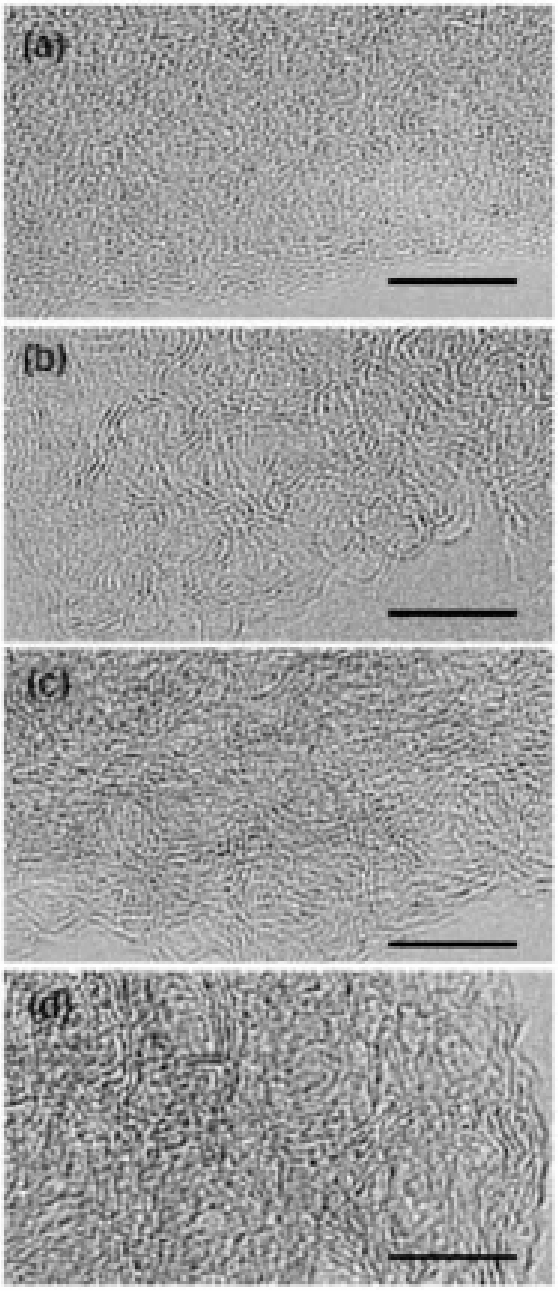

Figure 4. TEM micrographs of TiC-CDC synthesized at 400°C (a), 800°C (b), 1000°C (c), and 1200°C (d); scale bar 5 nm. At 400°C, the carbon produced is mostly amorphous. As the temperature increases to 800°C and above, thin non-planar graphitic fringes are seen. Planarization of graphite fringes and increase in their length can be seen at higher temperatures.

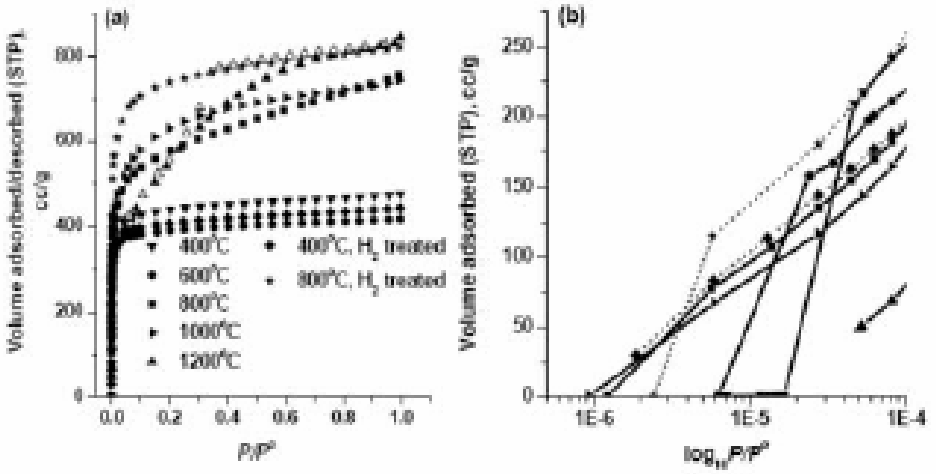

Figure 5. Argon adsorption isotherms at -195.8°C of TiC-CDC at different synthesis temperatures (a), and semilogarithmic scale plot (b) showing the low pressure region of (a). All isotherms except for sample chlorinated at 1200°C were reversible with no hysteresis between adsorption and desorption isotherms. Hollow symbols indicate desorption for the 1200°C sample.

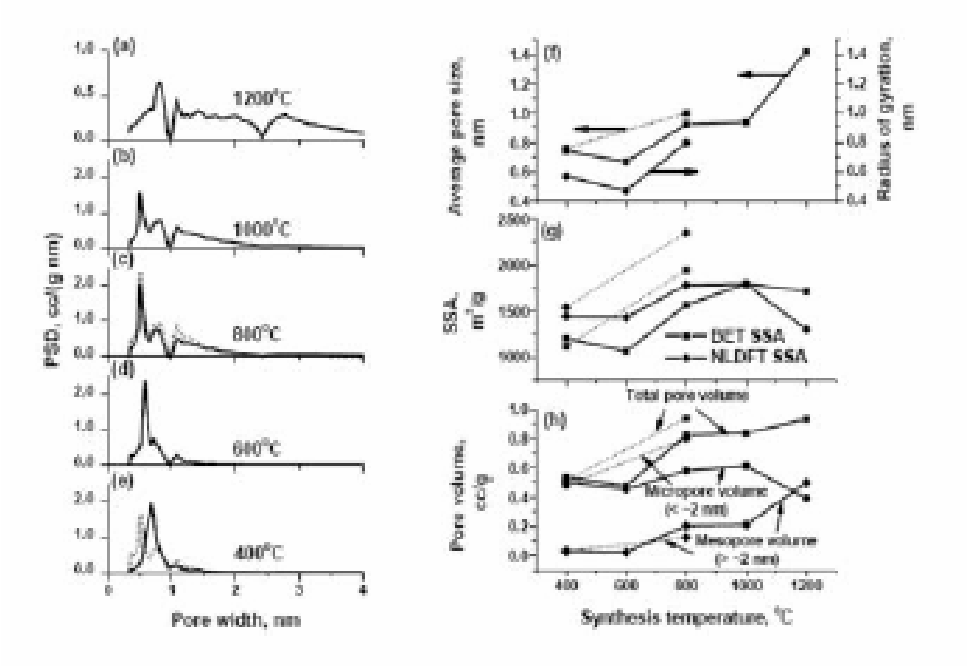

Figure 6. PSDs of TiC-CDC synthesized at a) 1200°C, b) 1000°C, c) 800°C, d) 600°C, and e) 400°C. As synthesis temperature increases, the PSDs become wider and shift towards larger pore sizes. f) Weighted average pore size and radius of gyration, g) BET and NLDFT SSA, and h) pore volume for different synthesis temperatures. Dotted lines indicate hydrogen treated samples.

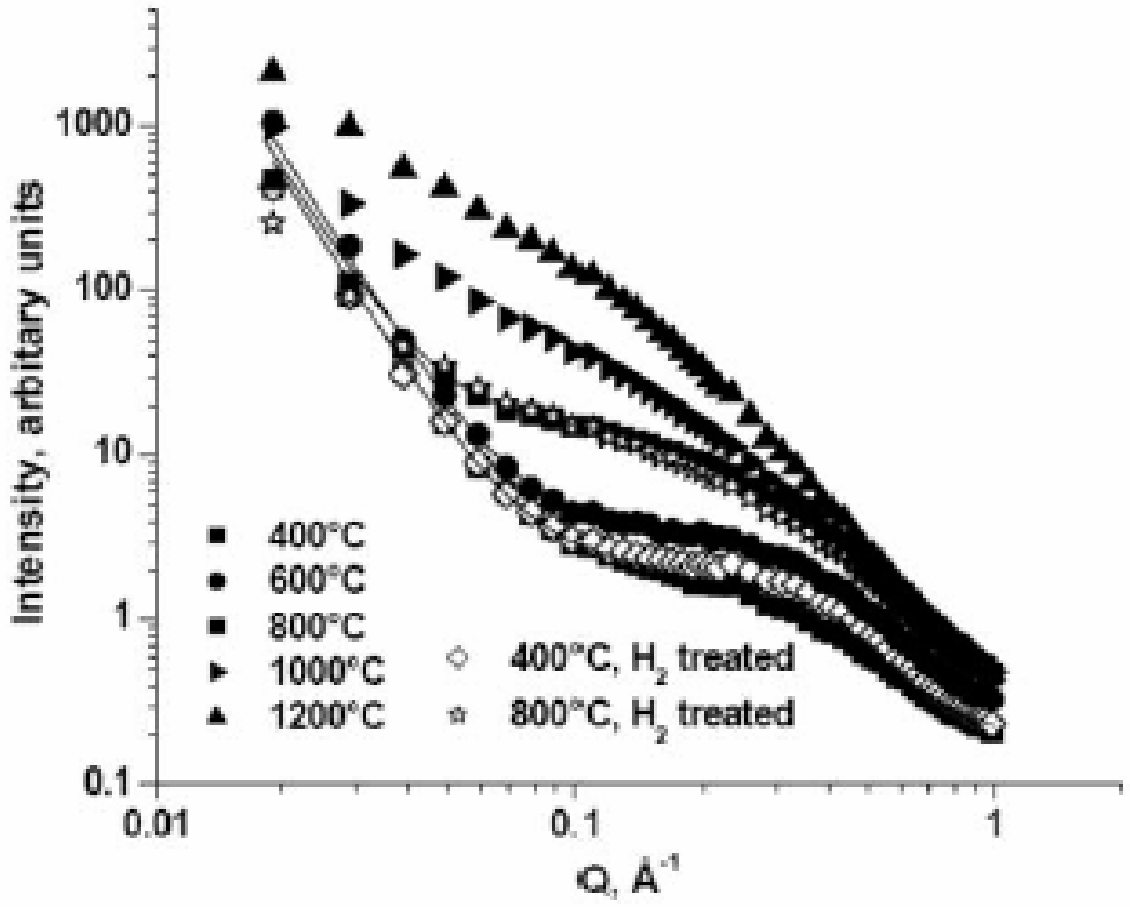

Figure 7. SAXS profiles of TiC-CDC synthesized at different temperatures (displaced vertically for clarity). Solid symbols stand for as-produced and hollow for hydrogen-treated samples. Solid lines are fits described in the text. Note the strong qualitative differences between low- and high-T profiles. Open symbols show that hydrogen annealing leads to negligible changes in pore morphology despite the notable improvement in storage capacity (see text).

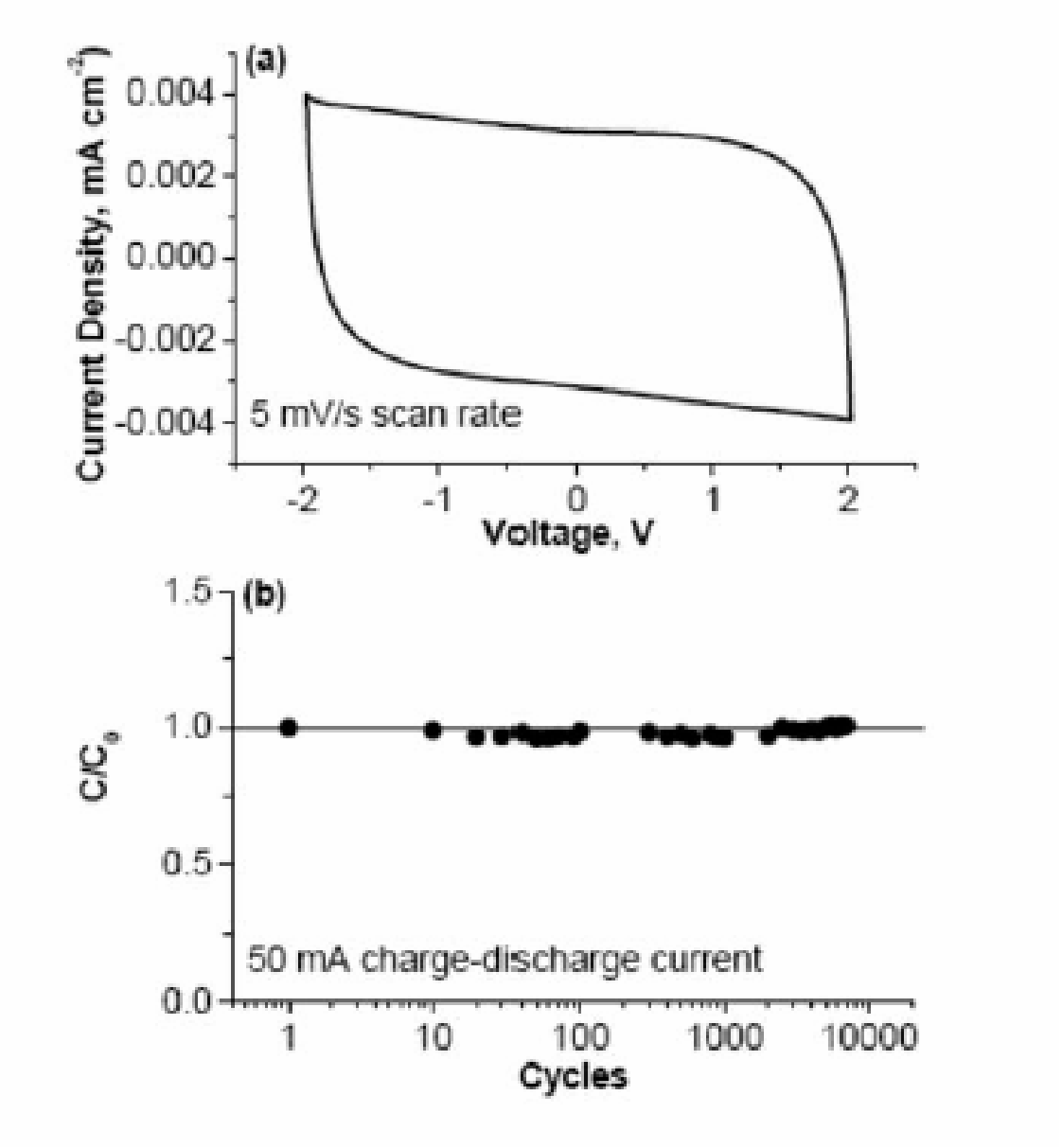

Figure 8. (a) Cyclic voltammogram (CV) of 600ºC TiC-CDC recorded at a sweep rate of 5 mV/s. (b) Galvanostatic cycling experiments performed at 50 mA show no appreciable change in specific capacitance (C_o) versus the specific capacitance calculated during the first cycle (C). The absence of peaks in the CV and lack of capacitance degradation during cycling highlight the purity of CDC produced.

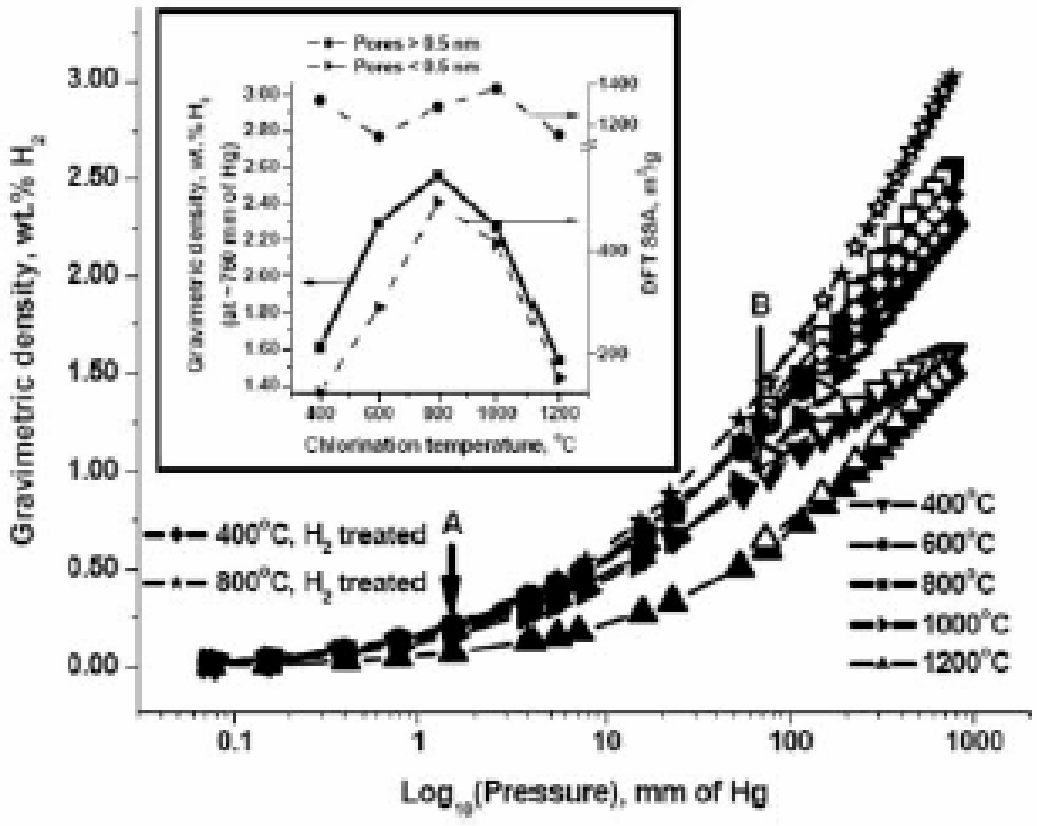

Figure 9. Hydrogen isotherms in semi-logarithmic scale of CDCs synthesized at 400, 800, 1000, and 1200°C. The sorption at -195.8°C was completely reversible with no hysterisis between adsorption (solid symbols) and desorption (empty symbols) isotherms. A correlation between SSA of pores smaller than 0.5 nm and hydrogen uptake (inset) is clearly seen. Hydrogen treated TiC-CDC showed higher hydrogen sorption than untreated samples.

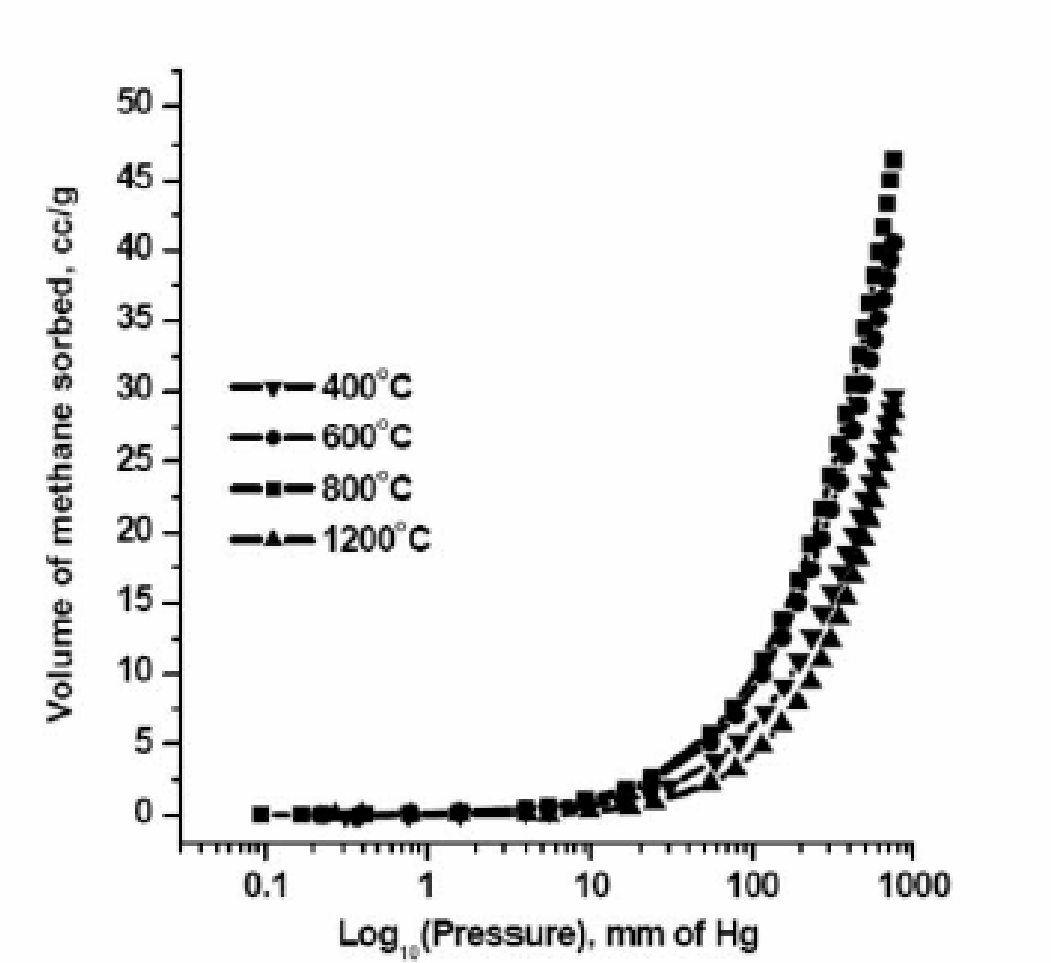

Figure 10. Methane sorption isotherms in semi-logarithmic scale of CDCs synthesized at 400, 600 and 1200°C.